NETWORK REWIRING MODELS

T. S. Evans

Theoretical Physics, Blackett Laboratory, Imperial College London
South Kensington campus, London, SW7 2AZ, UK

A. D. K. Plato

Institute for Mathematical Sciences, Imperial College London,
53 Prince's Gate South Kensington, London, SW7 2PG, UK

Abstract. Recently we showed that a simple model of network rewiring could
be solved exactly for any time and any parameter value. We also showed that
this model can be recast in terms of several well known models of statistical
physics such as Urn model and the Voter model. We also noted that it has been
applied to a wide range of problems. Here we consider various generalisations
of this model and include some new exact results.

1. **Introduction.** Graphs with a constant number of edges and vertices but which
evolve by rewiring those edges are a classic network model as exemplified by Watts
and Stogatz [21] ([18, 17] provide further examples). Such network evolution may
also be recast as other types of statistical physics models (for example see [10, 5, 14,
20]). As many real systems are effectively of constant size, non growing networks
can also be used to model a wide range of data: the transmission of cultural artifacts
such as pottery designs, dog breed and baby name popularity (as in [11, 12, 2, 1]),
the distribution of family names in constant populations, and the diversity of genes.
In this paper we look at various extensions to a model of network rewiring for which
an exact solution [8] was presented at ECCS06 [6] and in more detail in [7].

2. **The model.** We will study the rewiring of a bipartite graph consisting of E
'individual' vertices connected by one edge only to any one of N 'artifact' vertices,
as shown in Fig. 1. At each time step two choices are made. With probability
Π_R an individual is chosen. This individual is connected by its single edge to an
artifact which we will refer to as the 'departure' artifact. It is the artifact end
of this edge which is to be rewired, to be moved from the departure artifact to
an 'arrival' artifact. The latter is chosen with probability Π_A. Only after the
departure and arrival artifacts have been chosen is the network altered. Note we
do not explicitly exclude the possibility that the departure and arrival artifacts are
the same. The individual vertices always retain one edge while the degree k of the
artifact vertices is changing in time, only its average degree $\langle k \rangle = E/N$ is constant.
It is the distribution of the artifact vertices at time t, $n(k,t)$, and its probability
distribution $p(k,t) = n(k,t)/N$, that we study.

This process can be viewed in many ways [7] other than the bipartite network
presented here. Projections onto the rewiring of unipartite graphs are considered
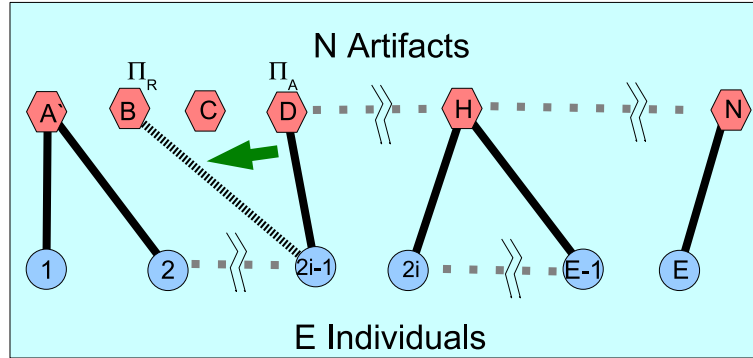
FIGURE 1. The bipartite graph has E 'individual' vertices, each with one edge. The other end of the edge is connected to one of N 'artifact' vertices. If the degree of an artifact vertex is k then this artifact has been 'chosen' by k distinct individuals. At each time step a single rewiring of the artifact end of one edge occurs. An individual is chosen (number $(2i-1)$ here) with probability Π_R which gives us the departure artifact (here D). At the same time the arrival artifact is chosen with probability Π_A (here labelled B). After both choices have been made the rewiring is performed (here individual $(2i-1)$ switches its edge from artifact D to B).

in Section 3. As we will see in Section 4, this model may be considered to be a particular generalisation of a basic Voter model. The terminology used in this paper comes when this process is used to model cultural transmission [11, 12, 2, 1, 8, 6, 7]. There the bipartite graph represents individuals who are choosing artifacts by either copying the choices made by another individual (preferential attachment) or by making their own innovation (random attachment). In this context the model has been used on data where there is no particular advantage in choosing one artifact over another, such as pottery designs, choice of dog breeds and baby name popularity [11, 12, 2, 1]. A more extensive review of the relationship to other models is given in [7].

The evolution of the degree distribution in the mean field approximation is described by the master equation [8, 6, 7]

$$
\begin{aligned}
n(k&, t+1) - n(k, t) \\
=\ & n(k+1, t)\Pi_R(k+1, t)\left(1 - \Pi_A(k+1, t)\right) \\
& -n(k, t)\Pi_R(k, t)\left(1 - \Pi_A(k, t)\right) - n(k, t)\Pi_A(k, t)\left(1 - \Pi_R(k, t)\right) \\
& +n(k-1, t)\Pi_A(k-1, t)\left(1 - \Pi_R(k-1, t)\right) .
\end{aligned}
\tag{1}
$$

For our physical problem the removal probability must always satisfy $\Pi_R(k=0) = 0$ and $\Pi_R(k=E) = 1$. In addition for physical solutions we must have $n(k, t) = 0$ if $k < 0$ or $k > E$. The presence of the factors of $(1 - \Pi)$ ensure that if the degree distribution initially satisfies its physical boundary condition, $n(k, t = 0) = 0$ if $k < 0$ or $k > E$, then this boundary condition is automatically satisfied at all

times[1]. The factors of $(1 - \Pi)$ are not seen in the master equations of the literature [18, 17, 10, 3] and correspond to events where the arrival and departure artifacts are chosen to be the same[2].

In general the master equation (1) gives only an approximation to the evolution of the ensemble averaged degree distribution. The terms in the master equation (1) actually represent the average of various moments, products of the form $\langle n_\alpha(k)k^m/Z_\alpha \rangle$ where Z_α comes from normalisations associated with some probabilities. The average is an ensemble average over different configurations, labelled here by α. Unfortunately in the general case, the normalisation depends on the nature of each configuration α. This means that we can not in general factorise these expressions into $\langle n_\alpha(k)k^m \rangle \langle Z_{\alpha'}^{-1} \rangle$ or similar. Without this we can not reduce the master equation for the *average* degree distribution $n(k)$ into a set of coupled linear equations for the $n(k)$ values. The only case when the factorisation is possible is when the normalisations are made from constants of the motion and so $Z_\alpha lpah$ are independent of the configuration. The only such constants are N and E. The most general Π_R and Π_A which use only constant normalisations are

$$\Pi_R = \frac{k}{E}, \qquad \Pi_A = p_r\frac{1}{N} + (1 - p_r)\frac{k}{E}, \qquad (E \geq k \geq 0) . \tag{2}$$

We will restrict ourselves to these forms and therefore our analytic results give an *exact* result for the average degree distribution at each time [7].

We interpret the forms (2) as choosing our arrival edge with a mixture of preferential attachment (probability $(1 - p_r)$) and random attachment (probability p_r). When using (2) the removal artifact is found by choosing the artifact end of a randomly selected edge — 'preferential removal'. The use of probabilities proportional to k can emerge naturally through short range searches of many networks, since the probability of arriving at a vertex on a random graph is proportional to its degree [16, 4, 9].

Not only is the master equation exact for our chosen probabilities (2) but the exact solution for the degree distribution $n(k, t)$ may be found for any finite parameter value. This may be done in terms of $(E + 1)$ eigenfunctions $\omega^{(m)}(k)$ and their corresponding generating functions $G^{(m)}(x)$

$$n(k, t) = Np(k, t) = \sum_{m=0}^{E} c_m(\lambda_m)^t \omega^{(m)}(k), \tag{3}$$

$$G(x, t) := \sum_{k=0}^{E} x^k n(k, t) = \sum_{m=0}^{E} c_m(\lambda_m)^t G^{(m)}(x), \tag{4}$$

$$G^{(m)}(x) := \sum_{k=0}^{E} x^k \omega^{(m)}(k). \tag{5}$$

---

[1]For this to be true it is absolutely vital that we have the factors of $(1 - \Pi_R(k))$ to ensure that with the condition $\Pi_R(k = E) = 1$ we do not include processes where an artifact with E edges is lost because we are adding another edge (the third term in (1) for $k = E$).

[2] These events occur with probability $(\Pi_R\Pi_A)$. Since the network is unchanged by such events, we must exclude such events from the evolution of $n(k, t)$ and the factors of $(1 - \Pi)$ implement this. It is an approximation to drop these terms. In our model this is not justified for certain parameter values.

The solution is found to consist of simple combinations of the Hypergeometric function $F(a, b; c; x)$ [7]

$$G^{(m)}(x) \quad = \quad (1-x)^m F(a+m, b+m; c; x) \tag{6}$$

$$= \quad (1-x)^m \sum_{l=0}^{E-m} \frac{\Gamma(a+m+l)\Gamma(b+m+l)\Gamma(c)}{\Gamma(a+m)\Gamma(b+m)\Gamma(c+l)(l!)} x^l \tag{7}$$

where

$$a = \frac{p_r}{1-p_r}\langle k \rangle\,, \qquad b = -E\,, \qquad c = 1 + \frac{p_r}{1-p_r}\langle k \rangle - \frac{E}{1-p_r}. \tag{8}$$

The corresponding eigenvalues are found to be

$$\lambda_m = 1 - m\frac{p_r}{E} - m(m-1)\frac{(1-p_r)}{E^2}, \qquad E \geq m \geq 0\,, \tag{9}$$

and these satisfy $\lambda_m > \lambda_{m+1}$ except for $p_r = 0$ when $\lambda_0 = \lambda_1 = 1$.

There is a unique long time equilibrium distribution which can be of one of two phases, as Fig. 2 shows. For $0 \leq p_r \lesssim E^{-1}$ we get a condensate where almost all individuals attach to a single artifact. For p_r greater than $(1/E)$ there is no such condensate. For low values, $E^{-1} \ll p_r \lesssim (1 + \langle k \rangle)^{-1}$, the degree distribution is a power law of slope $\gamma = 1 - (p_r\langle k \rangle/(1 - p_r)) \leq 1$, with an exponential cutoff $n(k) \approx k^{-\gamma}e^{-\zeta k}$ ($\zeta = -\ln(1-p_r)$). For larger[3] values of p_r the distribution is shaped like the binomial distribution which is the distribution at $p_r = 1$. The transition between condensate and non-condensate regimes is smooth except in the $E \to \infty$ limit.
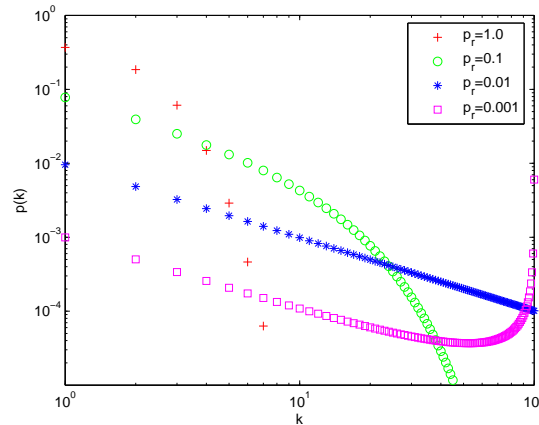

FIGURE 2. Plots of the degree probability distribution function $p(k) = n(k)/N$ for $N = E = 100$ and various $p_r = 1$ (red crosses), $10/E$ (green circles), $1/E$ (blue stars) and $0.1/E$ (magenta squares). Note that $p_r = 1/E$ is almost a pure power law for all values of k while $p_r = 1$ is a binomial distribution.

---

[3]Note that the largest physical value of p_r is actually $N/(N-1)$. Values of p_r greater than one are interpreted in terms of a repulsion process, a third term proportional to $(E-k)$ in (2). Such a process leaves the functional form for Π_A unchanged and the analytic results still hold exactly but the maximum physical value for the parameter p_r is now larger than one.

Using the fact that the number of artifacts N and the number of edges E are constant gives $c_0 = N$ and $c_1 = 0$ so that the eigenmode numbered one ($m = 1$) never contributes. Thus the approach to equilibrium of most quantities occurs on a timescale

$$\tau_2 = -[\ln(\lambda_2)]^{-1} \tag{10}$$

as illustrated in Fig. 3. This means that if we have rewired most of the edges once and almost never used random attachment, i.e. $p_r \lesssim E^{-1}$, then the approach to equilibrium is slow, $\tau_2 = O(E^2)$. However for other cases, $p_r \gg E^{-1}$, the small amount of randomness gives a rapid approach to equilibrium after every edge has been rewired just a few times. The initial conditions determine the remaining c_m ($m > 1$).
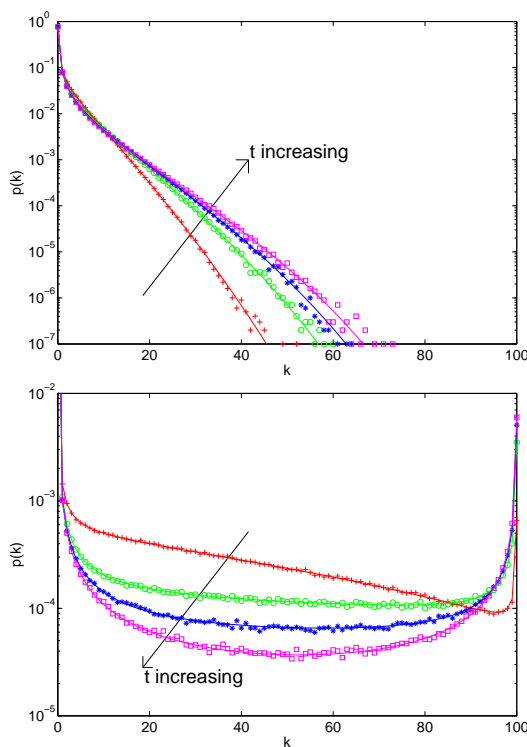

FIGURE 3. Plots of $p(k)$ from simulations (data points) and the exact analytic results (lines) for $E = N = 100$ with $p_r = 10/E$ on the left and $p_r = 0.1/E$ on the right. The results are shown at four different times: $t \approx \tau_2$ (red, crosses), $t \approx 2\tau_2$ (green, circles), $t \approx 3\tau_2$ (blue, stars) and to equilibrium (magenta, squares). The initial configuration has one edge per artifact. The data points are averages over 10^5 runs while the lines are the exact analytic results.

Of particular interest are the homogeneity measures $F_n(t)$ which are the probability that n randomly chosen but distinct edges all share the same artifact. These

are given by

$$F_n(t) \quad := \quad \frac{\Gamma(E+1-n)}{\Gamma(E+1)} \left. \frac{d^n G(x,t)}{dx^n} \right|_{x=1} \tag{11}$$

$$= \quad \sum_{k=0}^{E} \frac{k}{E} \frac{(k-1)}{(E-1)} \cdots \frac{(k-n+1)}{(E-n+1)} n(k,t) . \tag{12}$$

The properties of the Hypergeometric function mean we can express the solutions in terms of fixed fractions of a large number of fixed Gamma functions with all the dependence on time and the initial conditions is carried by factors of $c_m(\lambda_m)^t$. Also the n-th homogeneity measure $F_n(t)$ has contributions only from the eigenfunctions $m \leq n$.

For instance the most useful homogeneity measure is $F_2(t)$:

$$F_2(t) \quad = \quad F_2(\infty) + (\lambda_2)^t \left(F_2(0) - F_2(\infty) \right) , \tag{13}$$

$$F_2(\infty) \quad = \quad \frac{1 + p_r(\langle k \rangle - 1)}{1 + p_r(E-1)} , \tag{14}$$

while the initial conditions set $F_2(0)$.

3. **Phase transitions of unipartite graphs in real time.** The construction of Molloy and Reed [15] gives a unipartite graph of a given degree distribution but is otherwise random. In terms of our bipartite graph this is equivalent to taking pairs of individual vertices and merging the edge ends ('stubs') coming out of these individual vertices. The individual vertices are then thrown away. This is illustrated in Fig. 4.

The rewiring of our bipartite model is then equivalent to a rewiring of the projected unipartite graph with the same linear attachment and removal probabilities, also illustrated in Fig. 4. Since the degree distribution of our artifact vertices is
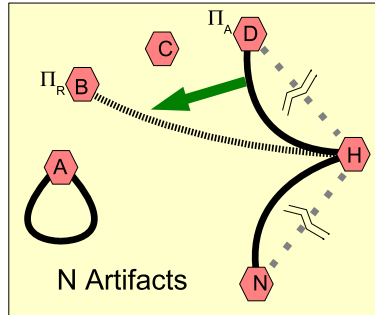

FIGURE 4. One projection of the bipartite graph of Fig. 1 onto this undirected unipartite graph. Let $a(i)$ be the artifact vertex connected to the individual vertex i in the bipartite graph. Then we take pairs of individual vertices $(2i)$ and $(2i-1)$ in the bipartite graph and connect their associated artifacts $a(2i-1)$ and $a(2i)$ in the undirected graph. The rewiring event of Fig. 1 now become a rewiring of the (D,H) edge to a (B,H) edge.

also the degree distribution of the unipartite graph, all our results can be applied

directly to such graphs. For instance for $p_r = 1$ we capture the degree distribution of the original Watts and Stogatz model[4] [21].

Analytic expressions for the global properties of such random graphs in the infinite N limit depend on a ratio, z, of the second and first moments of the degree distribution [16, 4, 9, 15]

$$z(t) := \frac{\langle k^2 \rangle}{\langle k \rangle} - 1 = (E-1)F_2(t) . \tag{15}$$

There is a phase transition in the properties of such infinite random graphs at $z = 1$. This occurs when there is one tadpole (an edge connected at both ends to the same vertex) in the unipartite graph. In particular for $z > 1$ the average distance between two vertices in the giant component, $\langle l \rangle$, may be estimated to be[5] [9]

$$\langle l \rangle = \frac{-2\langle \ln(k) \rangle + \ln(E) - \gamma_E}{\ln(z)} + \frac{3}{2} , \qquad \gamma_E \approx 0.5772 . \tag{16}$$

For simplicity we consider graphs where $N = E$ which start with each artifact connected to only one individual so $n(k, t=0) = E\delta_{k,1}$. The projected unipartite graph has $\langle k \rangle = 1$ and initially $F_2(0) = z(0) = 0$. If $p_r \gg O(E^{-1})$ then the equilibrium configuration is reached quickly in $t \sim O(\tau_2) = O(E)$ steps. Only when we start to get a high degree node, so a condensate is forming and $p_r \lesssim O(E^{-1})$, do we get a slower approach to equilibrium on a time scale $\tau_2 = O(E^2)$. The phase transition in infinite random graphs occurs at $z = 1$. In our case, our projected graphs start from $z(0) = 0$ but they reach $z = 1$ very quickly at $t_1 \approx E/2$ unless $(1 - p_r) \gg O(E^{-1})$. That is even if the evolution to the equilibrium distribution is slow, provided a reasonably large degree node exists, i.e. there is significant amount of copying, a large component emerges in the projected unipartite graph quickly, typically at $t_1 \approx E/2$, since

$$t_1 = \frac{\ln(1 - ((E-1)F_2(\infty))^{-1})}{\ln(\lambda_2)} , \tag{17}$$

$$\approx \frac{E}{2(1 + p_r(\langle k \rangle - 1))} \cdot \frac{E}{E-1} , \qquad (1 - p_r) \gg \frac{1}{E} . \tag{18}$$

The numerical results for the evolution of the properties of the projected unipartite graph are shown in Fig. 5. The parameter z reaches the value 1 at $(t_1/E) \approx 0.5 \pm 0.0002$ as expected. This is close to, but not exactly equal to, $(t_p/E) = 0.535 \pm 0.005$, where t_p is the time at which the average distance and diameter of the largest component peak. The second derivative in time of the number of vertices in the largest component also suddenly switches sign at exactly the same time t_p. The value of z at this time is $z(t_p) = 1.06 \pm 0.01$.

Motivated by the approximate expression for the distance in the largest component of a large random graph (16), we find that the inverse distance for the

---

[4]Strictly speaking we choose a random edge to rewire while Watts and Stogatz [21] rewired in a systematic manner.

[5]This formula must be adapted from [9] to take account of the existence of vertices of zero degree. Analytic derivations of such global properties use an ensemble of graphs over which there is always a finite probability of getting from any one vertex of degree $k_i > 0$ to a vertex of degree $k_j > 0$ in a finite number of steps. In any one graph this need not be true. On the other hand numerically we measure the average distance in the largest component of *one* graph considering only vertices in the largest component. We then average this result over the ensemble of graphs. Numerical evidence suggests that this numerical measurement has the same qualitative behaviour as the analytic formula.
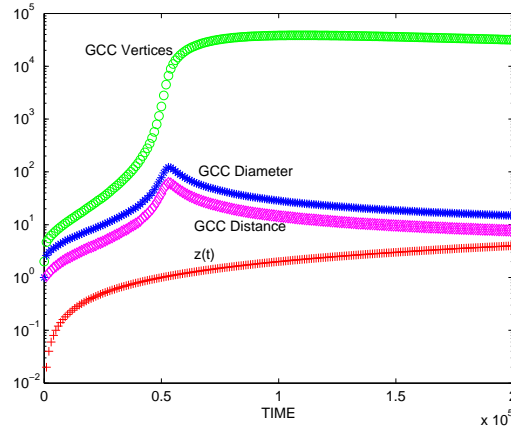
FIGURE 5. Properties of the undirected random graph formed using a Molloy-Reed type projection [15]. The underlying bipartite graph has $N = E = 10^5$ starting from $F_2(0) = 0$ and rewired with pure copying ($p_r = 0$). Results are calculated for each instance and then averaged over a total of 1000 runs.

.

parameters used in Fig. 5 is well fitted by the form $a \ln(z - 0.06) + b + cz + dz^2$ but with different values either side of the peak time[6]. The fit is shown in Fig. 6. The deviations from the predicted $z = 1$ transition point seem to be finite size effects. The peaks are sharper and closer to $z = 1$ as the network get larger[7] but with the same $\langle k \rangle$, p_r and $F_2(0) = 0$.

The network shown in Fig. 5 is evolved with pure copying ($p_r = 0$) so in this case the equilibrium distribution, a complete condensate $F_2 = 1$, will emerge only on a long time scale of $\tau_2 = -[\ln(1 - 2E^{-2})]^{-1} \sim O(E^2)$.

One way to look at this transition is to use the interpretation of the model in terms of cultural transmission [11, 12, 2, 1, 8, 6, 7]. In this case the bipartite graph represents individuals who are choosing artifacts by either copying the choices made by another individual (preferential attachment) or by making their own innovation (random attachment). Suppose we now imagine that each person has two copies of an artifact. The unipartite graph is then one expression of the relationship between objects as defined by the choices made by individuals. For instance one could imagine asking people to categorise their two favourite pairs of shoes and each artifact could represent a different category, e.g. one artifact might represent black leather lace up shoes. The unipartite projection gives a metric in artifact space as defined by the choices made by the individuals. The phase transition in the unipartite network then marks the point where the individuals have reached

---

[6]For early times, $z < z(t_p)$, we have $a = -0.107 \pm 0.006$, $b = 0.30 \pm 0.02$, $c = -0.42 \pm 0.04$ and $d = 0.14 \pm 0.03$ (fit excluded the four points with lowest z values) while for late times and $z > z(t_p)$, we have $a = +0.85 \pm 0.02$, $b = 0.019 \pm 0.02$, $c = -0.002 \pm 0.06$ and $d = 0.0008 \pm 0.0003$. These fits have $R^2 = 0.9995$ and $R^2 = 0.9999$ respectively and errors are at 95% confidence level. However a polynomial works almost as well, at least near $t = t_p$.

[7]For $N = E$ and $p_r = 0.0$, we find: $N = 10^3$, $t_p/E = 0.66 \pm 0.04$; $N = 10^4$, $t_p/E = 0.57 \pm 0.01$; $N = 10^5$, $t_p/E = 0.535 \pm 0.005$. Estimated from an ensemble of 1000 independent runs for each value of $N = E$.
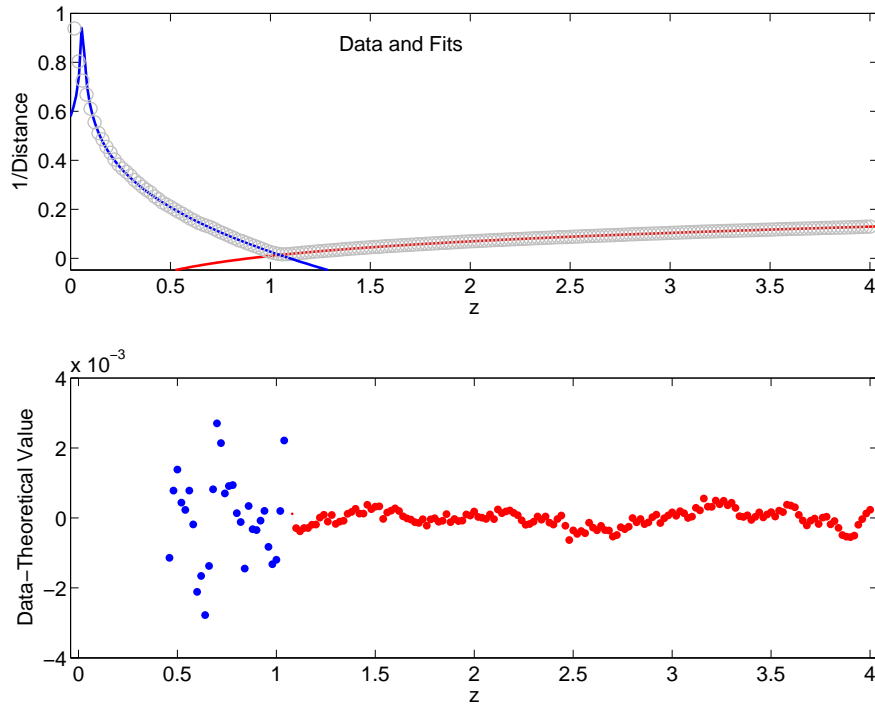
FIGURE 6. The inverse distance of the largest component for the same projected networks as in Fig. 5. The points are the data (errors are smaller than the symbol size) and the lines are the best fits to the form $a \ln(z - 0.06) + b + cz + dz^2$. The lower figure shows the residuals illustrating the good fit.

some sort of consensus as the artifacts now form a Giant Connected Component given the metric provided by the individuals' choices.

4. **Voter models and individual networks.** One generalisation of our rewiring model is to add a second graph connecting the individual vertices. We will this the Individual graph and this is illustrated in Fig. 7. When an individual rewires using preferential attachment they copy the artifact chosen by one of their neighbours in the Individual network. With $p_r = 0$ and $N = 2$ we obtain the basic Voter model [14, 20], which is related to some models of language evolution [19]. Our model corresponds to having a complete graph for the individual network but with the addition of a random rewiring process, $p_r > 0$, and an arbitrarily large number of choices, $N \geq 2$. Neither of these cases is studied in the Voter model literature where the focus is on different types of individual networks and any analytic results are only available for the $E \to \infty$ limit [20][8].

---

[8]For $p_r > 0$ we can think of our model as including two graphs. The first, as mentioned above, is a graph connecting Individuals. Preferential rewiring is done by performing a random walk of length one on this graph, and copying the choice of the resultant Individual. The second graph connects the Artifacts [7]. If this graph is a complete graph (with tadpoles) then a random walk on the graph gives the random attachment p_r term appearing in Π_A of (2). One may imagine many practical problems where the Artifact network is not so trivial. For this paper, however, we only consider the case of a complete Artifact graph.
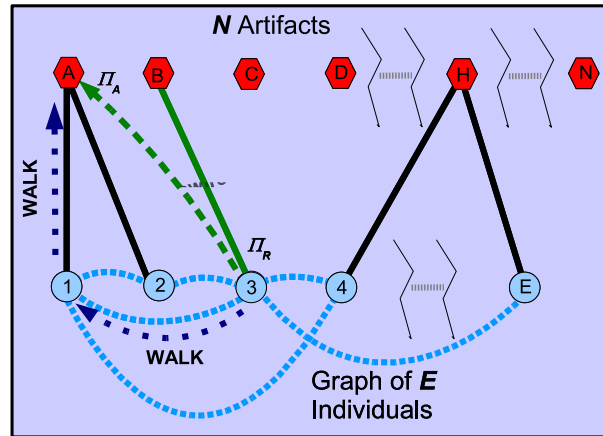
FIGURE 7. The bipartite network with an Individual graph added. This is a network consisting of the individual vertices connected by the the light blue dashed lines shown below the individual vertices. Illustrated is a rewiring event where individual **3** copies the artifact choice of individual **1** so that the **3-B** edge is rewired to become a **3-A** edge. However instead of finding the arrival artifact **A** by preferential attachment, this is now found by making a random walk on the individual graph followed by a final step on the bipartite graph, here shown by the dark blue arrowed lines annotated with 'walk'.
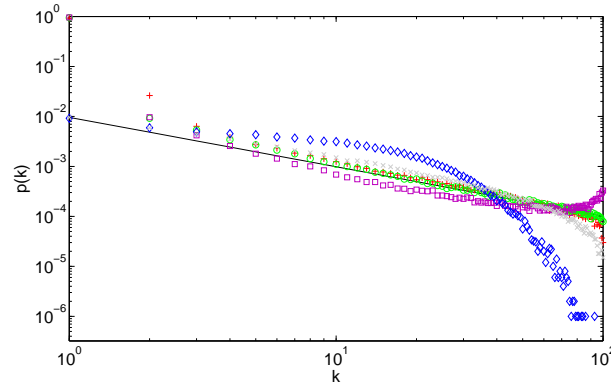

FIGURE 8. Equilibrium artifact degree distribution $p(k)$ for different Individual graphs of 100 vertices and average degree 4: Erdős-Réyni (red pluses), Exponential (green circles), Barabási-Albert (purple squares), periodic lattices of two (grey crosses) and one (blue diamonds) dimension. The line is the analytic result for a complete Individual graph while the other results are taken over an ensemble of 10^4 Individual graphs. $N = E = 100$, $p_r = 1/E$.

Results for the equilibrium distribution show that it is qualitatively unchanged by the type of individual graph[9] except for the case of a one dimensional ring, as shown in Fig. 8.

---

[9]In this article, the lattices are cubic ($\mathbb{Z}^d$). In Fig. 8 next-to-nearest and nearest neighbours are connected in the one-dimensional ring. In all other cases the only nearest neighbours connected in

We will use two quantities to study the behaviour of the model. Our quantity F_2 of (12) is a measure of the global homogeneity. An equivalent measure which takes account of the local properties of the Individual network is the average interface density, $\langle \rho \rangle$, the probability that any two individual vertices connected by the Individual graph have a different artifact. If the graph is complete or if the Individual graph is ignored ($p_r = 1$) then from (14) we have $\langle \rho \rangle_t = 1 - F_2(t)$. Otherwise for two reasons we expect that $\langle \rho \rangle_t \neq 1 - F_2(t)$ and that both would both differ from value obtained for a complete Individual graph as derived from (14). First because of the explicit reference to the Individual graph in the definition of $\langle \rho \rangle_t$ but not in F_2. Second, the structure imposed by the Individual graph will, in general, effect both the evolution timescale and, for $p_r > 0$, equilibrium degree distributions as compared to the complete Individual graph case.

We can see these differences if we compare the equilibrium values reached on lattices of different dimensions but with some randomness present (otherwise $\langle \rho \rangle_t = (1 - F_2(t))$ because both are zero). As Fig. 9 and table 1 show, the local and global homogeneity measures $\langle \rho \rangle$ and $(1 - F_2)$ are close to the analytic result for large dimension lattices with short network distances. As we take lattices of smaller dimension, F_2 gets much larger than the analytic result, and $\langle \rho \rangle$ much smaller. Table 2 shows a similar effect as we increase p_r.
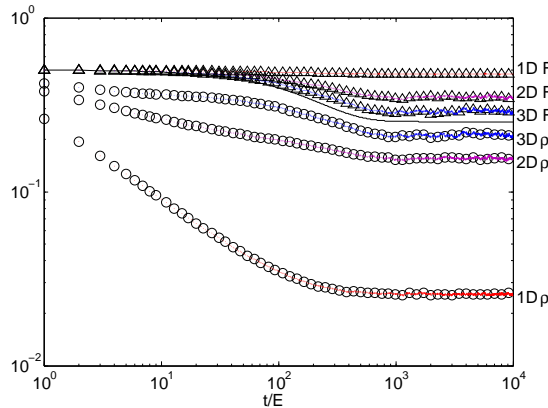

FIGURE 9. Homogeneity measures for various lattices against t/E. The black solid line represents the analytic $1 - F_2(t)$ for $N = 2$, $p_r = 1/E$ and $E = 729$. Numerical results for $1 - F_2(t)$ (triangle highlights) are plotted for 1-d (red), 2-d (purple) and 3-d (blue) regular lattices. The average interface densities $\langle \rho \rangle$ are plotted as circles. Averaged over 1000 runs.

The time scale of the approach to consensus is often studied in Voter models. If $p_r > 0$ there is no absolute consensus, so the approach to equilibrium may be measured by F_2 and ρ. If the Individuals are connected by a complete network, then these are controlled solely by the time scale associated with the second eigenvalue,

the lattice Individual graphs. The Exponential and Barabási-Albert graphs are connected graphs Individual graph degree distributions of $p_{\text{ind}}(k) \propto \exp\{-\zeta k\}$ and $p_{\text{ind}}(k) \propto [k(k+1)(k+2)]^{-1}$ respectively. The results also support the claim in [8, 6, 7] that some results for a Minority game played on an Erdős-Réyni graph can be understood in terms of our results for the rewiring model.

Dim	$t_0(F_2)/\tau_2$	$t_0(\rho)/\tau_2$	$1 - F_2(\infty)$	$\rho(\infty)$
1d	1.25 (3)	0.0241 (4)	0.47466 (2)	0.0261 (1)
2d	1.19 (1)	0.74 (1)	0.3494 (1)	0.1558 (1)
3d	1.10 (1)	1.06 (1)	0.2898 (1)	0.2120 (1)

TABLE 1. Table of time scales and the limiting value of the evolution of $1-F_2$ and ρ where the Individual graphs are periodic lattices with nearest neighbour connections only. The complete graph has $1 - F_2(t = \infty) \approx 0.25017$ and $\tau_2 \approx 1.3295 \times 10^5$. Extracted from the data of Fig. 9 by fitting to $a \exp(-t/t_0) + c$ with the estimated error in the last digit give by the numbers in brackets.

τ_2 of (10). For general Individual networks the evolution of the global F_2 or local $\langle \rho \rangle$ takes the same form as (14), $a \exp(-t/t_0) + c$. However, as one might expect, the formation of small patches of consensus between nearest neighbours, measured by $\langle \rho \rangle$, happens faster than the emergence of a global consensus, as measured by F_2. This is accentuated if there is a large distance between individuals as the comparison between lattices of different dimensions in Fig. 9 and in table 1 show. Varying p_r also shows that local equilibration is faster than global but there does seem to be a marked difference between $p_r \ll 1/E$ and $p_r \gtrsim 1/E$ as table 2 and Fig. 10 show. For $p_r E \ll 1$, local equilibration is a little slower than occurs on complete graph. However for $p_r E \gtrsim 1$, this randomness brings local equilibrium an order of magnitude faster than was the case with a complete graph. It shows that a little bit of randomness can speed up local equilibration but not if an overwhelming consensus is going to emerge.
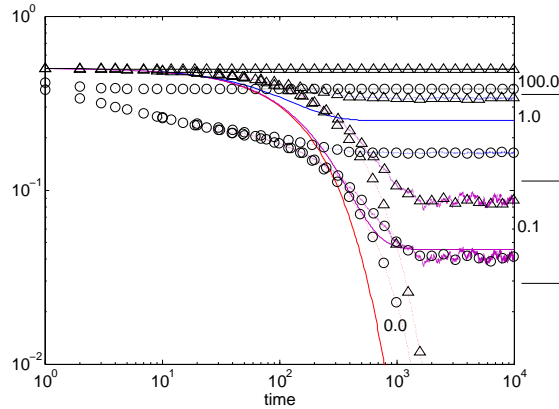

FIGURE 10. Plots of $(1 - F_2(t))$ (triangles) and $\langle \rho \rangle$ (circles) on a 2-d periodic lattice with side $L = 20$ and $N = 2$ for different attachment probabilities p_r. From top to bottom we have $p_r E = 100$ (black), $p_r E = 1.0$ (blue), $p_r E = 0.1$ (purple), and $p_r E = 0$ (red). Note that for a given set of parameters $(1-F_2(t))$ (triangles) are always higher than the $\langle \rho \rangle$ (circles). Solid coloured lines are the equivalent analytic results for $1 - F_2(t)$ on a complete graph. Averaged over 5000 runs for $p_r = 0$ and $p_r = 1/E$ and 1000 runs for all others. Data used for table 2.

$\frac{p_r}{E}$	τ_2	$t_0(F_2)/\tau_2$	$t_0(\rho)/\tau_2$	Exact $1-F_2(\infty)$	$1-F_2(\infty)$	$\rho(\infty)$
0	79999	2.131 (6)	1.8 (1)	0	0.0003 (3)	0.003 (3)
0.1	72743	1.988 (5)	1.81 (2)	0.04546	0.0827 (3)	0.0403 (4)
1	40050	1.34 (3)	0.15 (2)	0.25031	0.3375 (3)	0.167 (1)
10	7289	1.01 (6)	0.145 (3)	0.45558	0.47433 (4)	0.2634 (1)
100	794	0.7 (2)	0.40 (1)	0.49628	0.49712 (1)	0.3813 (1)

TABLE 2. Table of time scales in units of τ_2 and limiting value in units of the exact value for $c = F_2(t = \infty)$ for 400 individuals connected by a square lattice, using the data in Fig. 10. It was fitted to $a \exp(-t/t_0) + c$.
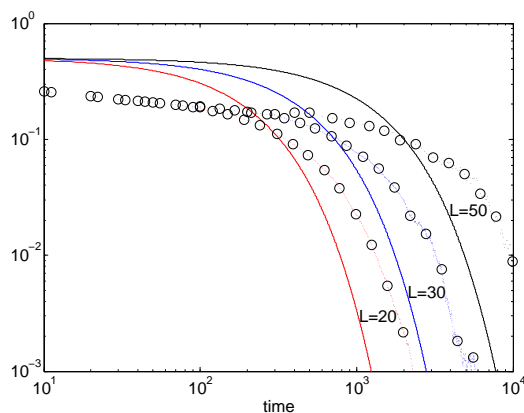

FIGURE 11. Numerical $\langle\rho\rangle$ (circles) on a 2-d periodic lattice with $N = 2$ and $p_r = 0$ for different sized lattices: from top to bottom at late times we have $L = 50$ (black), $L = 30$ (blue) and $L = 20$ (red). For comparison, analytic results for $(1 - F_2(t))$ (solid lines) on a complete graph are shown in the same order from top to bottom at late times. Averaged over 5000, 500 and 50 runs respectively. Data used for table 3.

In table 3 taken from Fig.s 11 and 12 we see that the time scales for the exponential decay obtained from fitting our data are roughly in line for the predictions made for the completion time in this model [14, 20, 13] on a lattice, $t_0 \sim O(E)$ for a one-dimensional lattice, $t_0 \sim O(\ln(E))$ in two dimensions. However some discrepancies suggest more work is needed.

The main result to draw from table 3 is that the evolution towards equilibrium, its time scale and final value, are independent of the number of artifacts. This is to be expected at small p_r given our linear attachment probabilities as this gives our model certain scaling properties [7]. Suppose we have the consensus emerging picking out one of our N artifacts and we merge the remaining $N - 1$ artifacts into one artifact. The probability of an individual copying the consensus artifact or one of the remaining artifacts is exactly the same as if we had a model with $N = 2$ and the same $(1 - p_r)$. The only difference is that when a random innovation event occurs, with probability p_r, the non-consensus artifacts are preferred to the single
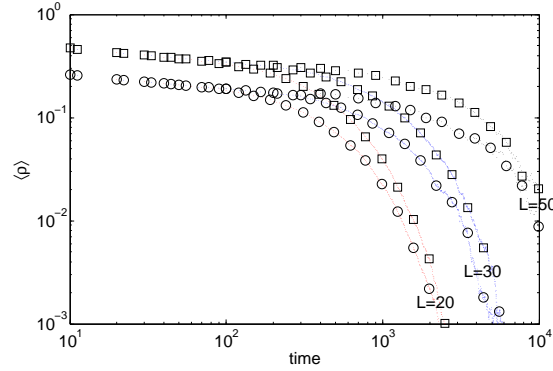
FIGURE 12. Plots of $\langle \rho \rangle$ on a 2-d periodic lattice with $p_r = 0$ for $N = 2$ (circles) and $N = 10$ (squares). At late times from top to bottom the lattice size is $L = 50$ (black), $L = 30$ (blue) and $L = 20$ (red). For each value of L the $N = 10$ is always higher than the $N = 2$ results. Averaged over 5000, 500 and 50 runs respectively. Data used for table 3.

			$N = 2$		$N = 10$	
Dim	E	τ_2	$t_0(1 - F_2)/\tau_2$	$t_0(\rho)/\tau_2$	$t_0(1 - F_2)/\tau_2$	$t_0(\rho)/\tau_2$
	100	4999.5	18.6 (1)	0.42 (2)	18.9 (1)	0.41 (1)
1d	200	19999	37.9	0.21 (1)	39.3	0.21 (1)
	400	79999	76.3	0.18 (1)	75.1	0.18 (1)
	1000	500000	115.7	0.069 (2)	137.8	0.070 (3)
	400	79999	2.131 (3)	1.8 (1)	2.109 (2)	1.8 (1)
2d	900	405000	2.3	2.1	2.3	2.1
	2500	3130000	2.8	2.1	2.8	2.1

TABLE 3. Table of time scales in units of τ_2 for E individuals connected by a one- or two-dimensional torus found by fitting the data to $a \exp(-t/t_0) + c$. For two and ten types of artifact, $p_r = 0$. The data used is shown in Fig.s 11 and 12. Where the error is known reliably, the number in brackets specifies the error in the last digit.

consensus artifact by a factor of $(N - 1)$. Thus for $N \gg 2$ the random events are more likely to destroy the emerging consensus than in the Voter model but *only* if $p_r \gg 0$. For the extreme case of $p_r = 0$ we see the expected lack of dependence on N in table 3. The only effect of increasing the number of artifacts in our results comes from starting from a homogeneous initial condition so $F_2 = 1/N$ which is further away from $F_2 = 1$ and consensus, see Fig. 13.

5. **Two types of individual.** Another variation of our original model is to introduce two types of individual, labelled X and Y, as shown in Fig. 14. At each time step we first pick which type of individual to update; with probability q_x we select at random one the X-type individuals. We rewire its artifact end, choosing its arrival artifact in one of three ways: at random, by copying the existing choice of one
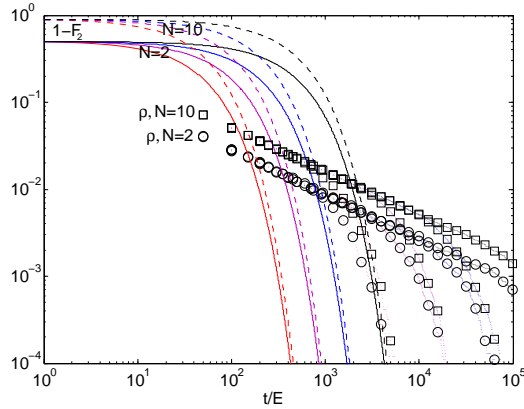
FIGURE 13. Plots of the analytic results for $(1 - F_2(t))$ (lines) on a complete graph compared with numerical results (symbols) for $\langle \rho \rangle_t$ on 1-d periodic lattices against t/E for $p_r = 0$ and for various values of E. In each case the plots move up and right as E is increased with $E = 100$ (red, far left), 200 (purple), 400 (blue) and 1000 (black, far right). The lower circles and the solid lines represent $N = 2$ while the higher squares and dashed lines are for $N = 10$. Data are averages over 1000, 1000, 500 and 100 runs for increasing lattice sizes respectively.

its own type of individual, or finally copying the existing choice made by a random individual of the opposite type. For edges attached to an individual of type X, we denote these probabilities as p_{rx}, p_{pxx} and p_{pxy} respectively, so $p_{rx} + p_{pxx} + p_{pxy} = 1$. These arrival probabilities may be different for the two types so we have four independent arrival probabilities (p's) and one departure probability (q's). Add in the freedom to choose different numbers of X and Y individuals, E_x and E_y, and N the number of artifacts, we find we have eight free parameters. The degree distribution is now $n(k_x, k_y; t)$, the number of artifact vertices which have k_x (k_y) edges to X (Y) type vertices at time t.

The question is can we solve this system analytically? By keeping our probabilities linear in degree and because our normalisations are constants of the evolution, our mean field equation is exact, for same reasons as in original model [7]. Writing in terms of the generating function $G(x, y, t) := \sum_{k_x=0}^{E_x} \sum_{k_y=0}^{E_y} x^{k_x} y^{k_y} n(k_x, k_y, t)$ we find that we can again split this into $(E_x + 1)(E_y + 1)$ eigenfunctions which we label with a pair of indices (MA):

$$G^{(MA)}(x, y) := \sum_{i=0}^{E_x} \sum_{j=0}^{E_y} (x - 1)^i (y - 1)^j f_{ij}^{(MA)}, \qquad (19)$$

where $f_{ij}^{(MA)}$ are constants. The eigenfunctions satisfy a two-dimensional second order PDE. We have not found a full solution but we can reduce this to a one-dimensional problem. Since we express our eigenfunctions in powers of $(x - 1)$ and $(y - 1)$, the eigenfunctions satisfy[10] $f_{ij}^{(MA)} = 0$ if $i + j < M$ for any integer

---

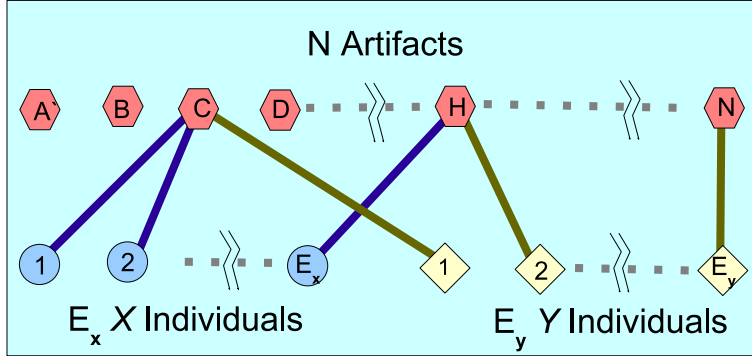[10] We use this to define our label M.

FIGURE 14. An illustration of the model with two types of Individual vertices. There are E_x type X individuals (circles) and E_y type Y Individuals.

$0 \leq M \leq E_x + E_y$. At the same time the equations for the coefficients $f_{ij}^{(MA)}$ and eigenvalues λ_{MA}, where $i + j = M$, involves no coefficients where $i + j > M$. Thus the label A indexes the allowed values of i and j given the constraint $i + j = M$. Finding the eigenvalues is therefore a matter of solving a set of $(\min(E_x, E_y) + 1)$ linear equations. This also gives the coefficients of the eigenfunctions for $i + j = M$. The remaining values $i + j > M$ may be found iteratively though this is generally a non-trivial problem.

However, we have seen that much information is encoded by the first and second moments of the degree distribution. The general homogeneity measures are given by

$$F_{mn}(t) := \frac{\Gamma(E_x + 1)}{\Gamma(E_x - m + 1)} \frac{\Gamma(E_y + 1)}{\Gamma(E_y - n + 1)} \left. \frac{\partial^{m+n} G(x, y; t)}{\partial x^m \partial y^n} \right|_{x=y=1} \tag{20}$$

So we only need the three second order homogeneity measures, $m + n = 2$. These have contributions only from the $i + j \leq 2$ coefficients and therefore only the $M \leq 2$ eigenfunctions contribute. The system of equations for such coefficients reduces to solving for the eigenvalues and eigenfunctions of a three dimensional system, which has an exact, if lengthy, algebraic solution. The basic results though are that the only equilibrium solution is given by the single $M = 0$ eigenfunction where $\lambda_0 = 1$, $f_{00}^{(0)} = N$, $f_{10}^{(0)} = E_x$, $f_{01}^{(0)} = E_y$, and the three coefficients $f_{20}^{(0)}, f_{11}^{(0)}, f_{02}^{(0)}$ satisfy

$$\mathbf{f}^{(0)} = \begin{pmatrix} f_{20}^{(0)} \\ f_{11}^{(0)} \\ f_{01}^{(0)} \end{pmatrix} = \mathsf{T}^{-1} \begin{pmatrix} \alpha_x(1 + a_x)(E_x - 1) \\ \alpha_x(d_x - a_x/E_x)E_y + \alpha_y(d_y - a_y/E_y)E_x \\ \alpha_y(1 + a_y)(E_y - 1) \end{pmatrix}, \tag{21}$$

$$\mathsf{T} := \begin{pmatrix} -2\alpha_x(1 + E_x^{-1}) & -\alpha_x d_x(1 - E_x) & 0 \\ -2\alpha_y d_y & \alpha_x \beta_x + \alpha_y \beta_y & -2\alpha_x d_x \\ 0 & -\alpha_y d_y(1 - E_y) & -2\alpha_y(1 + E_y) \end{pmatrix}, \tag{22}$$

$$a_x = \frac{p_{r_x}}{p_{p_{xx}}} \langle k_x \rangle, \ d_x = -\frac{p_{p_{xy}}}{p_{p_{xx}}} \frac{E_x^2}{E_y}, \ \alpha_x = \frac{q_x p_{pxx}}{(E_x)^2}, \ \beta_x = \frac{E_x(1 - p_{pxx})}{p_{pxx}}. \tag{23}$$

Switching labels $(x \leftrightarrow y)$ gives the similar y subscript parameters.

The $M = 1$ eigenfunctions again give no contribution to any physical quantity since the first moments are constant. The second moments are given in terms of the lowest coefficients of one of three $M = 2$ eigenfunctions, the $f_{20}^{(2A)}, f_{11}^{(2A)}, f_{02}^{(2A)}$ (assuming $E_x, E_y > 1$), which satisfy

$$(\lambda_{2A} - 1)\mathbf{f}^{(2A)} = \mathsf{T}\mathbf{f}^{(2A)}, \qquad \mathbf{f}^{(MA)} = \begin{pmatrix} f_{20}^{(MA)} \\ f_{11}^{(MA)} \\ f_{01}^{(MA)} \end{pmatrix}. \tag{24}$$

There is a large parameter space to investigate but there are a few obvious limits. First one can scale the probabilities in proportion to the number of edges of each type so $q_a = E_a/E$, $p_{ra} = p_r$, $p_{pab} = (1-p_r)E_b/E$ where $a, b \in \{x, y\}$, $E = E_x + E_y$. One can see then that the total degree distribution given by $G(x, x)$ is exactly as we had in the single type model. However we can now investigate the 'chemical equilibrium' as the distribution of X and Y types, given by derivatives of $G(x, 1)$ and $G(1, y)$ respectively, will evolve differently if the initial conditions are different for each type. Another simple example is where $p_{xx} = p_{yy} = 0$ which encodes the "complete bipartite graph example" of [20]. Our method allows one to extract exact expressions for the whole time evolution, not just order of magnitude estimates for the equilibration time.

6. **Conclusions.** In this paper we have looked at a variety of extensions to the basic network rewiring model of [8, 6, 7]. Studying the projection onto a unipartite graph gives us *exact* expressions for the time evolution of a finite sized system through a transition.

We have also shown that adding an Individual network leaves the qualitative behaviour of the model is unchanged in terms of F_2. However quantitative differences are highlighted by comparison against the case of a complete graph for which our previous analytic work [8, 6, 7] provides exact analytic results. What we learn from this model is that the consensus (the condensate) may not be perfect, $1 \gtrsim p_r E > 0$, and it may emerge very slowly $\tau_2 \sim O(E^2)$, but an effective consensus is always reached very quickly $t_1 \sim O(E)$.

Finally we have shown how some progress can be made on solving models with more than one type of edge. In particular we show how the various homogeneity measures F_{mn} may be found exactly.

REFERENCES

[1] R. A. Bentley, C. P. Lipo, H. A. Herzog and M. W. Hahn, *Regular rates of popular culture change reflect random copying*, Evolution and Human Behavior, **28** (2007).

[2] R. A. Bentley and S. J. Shennan, *Random copying and cultural evolution*, Science, **309** (2005).

[3] S. M. Dorogovtsev and J. F. F. Mendes, "Evolution of Networks," Oxford University Press, 2003.

[4] S. N. Dorogovtsev, J. F. F. Mendes and A. N. Samukhin, *Metric structure of random networks*, Nuc. Phys. B, **653** (2003), 307–338.

[5] M. R. Evans and T. Hanney, *Nonequilibrium statistical mechanics of the zero-range process and related models*, J. Phys. A, **38** (2005), R195–R240.

[6] T. S. Evans and A. D. K. Plato, *Exact solutions for models of cultural transmission and network rewiring*, Proceedings of ECCS06 [physics/0608052].

[7] ———, *Exact solution for the time evolution of network rewiring models*, Phys. Rev. E, **75** (2007).

[8] T. S. Evans, *Exact solutions for network rewiring models*, Eur. Phys. J. B, **56** (2007).

[9] A. Fronczak, P. Fronczak and J. A. Holyst, *How to calculate the main characteristics of random uncorrelated networks*, Science of Complex Networks: From Biology to the Internet and WWW; CNET 2004 (S.N. Mendes, J.F.F.Dorogovstev, A.Povolotsky, F.V. Abreu and J.G. Oliveira, eds.), vol. **776**, A.I.P., 2005.

[10] C. Godreche and J. M. Luck, *Nonequilibrium dynamics of urn models*, J.Phys. Condensed Matter, **14** (2002).

[11] M. W. Hahn and R. A. Bentley, *Drift as a mechanism for cultural change: an example from baby names*, Proc. R. Soc. Lon. B, **270** (2003).

[12] H. A. Herzog, R. A. Bentley and M. W. Hahn, *Random drift and large shifts in popularity of dog breeds*, Proc. R. Soc. Lon B (Suppl.), **271** (2004).

[13] P. L. Krapivsky, *Kinetics of monomer-monomer surface catalytic reactions*, Phys. Rev. A, **45** (1992).

[14] T. M. Liggett, "Stochastic Interacting Systems: Contact, Voter and Exclusion Processes," Springer-Verlag, New York, 1999.

[15] M. Molloy and B. Reed, *A critical point for random graphs with a given degree sequence*, Random Structures and Algorithms, **6** (1995), 161–179.

[16] M. E. J. Newman, S. H. Strogatz and D. J. Watts, *Random graphs with arbitrary degree distributions and their applications*, Phys. Rev. E, **64** (2001), 026118.

[17] J. Ohkubo, K. Tanaka and T. Horiguchi, *Generation of complex bipartite graphs by using a preferential rewiring process*, Phys. Rev. E, **72** (2005), 036120.

[18] K. Park, Y.-C. Lai and N. Ye, *Self-organized scale-free networks*, Phys. Rev. E, **72** (2005), 026131.

[19] D. Stauffer, X. Castello, V. M. Eguiluz and M. San Miguel, *Microscopic Abrams-Strogatz model of language competition*, Physica A, **374** (2007).

[20] V. Sood and S. Redner, *Voter model on heterogeneous graphs*, Phys. Rev. Lett., **94** (2005), 178701.

[21] D. J. Watts and S. H. Strogatz, *Collective dynamics of 'small-world' networks*, Nature, **393** (1998).

E-mail address: `t.evans@imperial.ac.uk`

E-mail address: `alexander.plato00@imperial.ac.uk`